Mon. Not. R. Astron. Soc. **000**, 000–000 (2008) Printed 14 February 2009 (MN LATEX style file v1.4)

Galaxy-Induced Transformation of Dark Matter Halos

Mario G. Abadi [1], Julio F. Navarro[2], Mark Fardal[3], Arif Babul[2] and Matthias Steinmetz[4]
[1] *Observatorio Astronómico de Córdobai and CONICET, Córdoba, Argentina*
[2] *Department of Physics and Astronomy, University of Victoria, Victoria, BC V8P 5C2, Canada*
[3] *Astronomy Department, University of Massachusetts at Amherst, MA 01003, US*
[4] *Astrophysikalisches Institut Potsdam, An der Sternwarte 16, Potsdam 14482, Germany*

ABSTRACT
We use N-body/gasdynamical cosmological simulations to examine the effect of the assembly of a central galaxy on the shape and mass profile of its surrounding dark matter halo. Two series of simulations are compared; one that follows only the evolution of the dark matter component of individual halos in the proper ΛCDM cosmological context, and a second series where a baryonic component is added and followed hydrodynamically. The gasdynamical simulations include radiative cooling but neglect the formation of stars and their feedback. The efficient, unimpeded cooling that results leads most baryons to collect at the halo center in a centrifugally-supported disk which, due to angular momentum losses, is too small and too massive when compared with typical spiral galaxies. This admittedly unrealistic model allows us, nevertheless, to gauge the maximum effect that galaxies may have in transforming their surrounding dark halos. We find, in agreement with earlier work, that the shape of the halo becomes more axisymmetric: post galaxy assembly, halos are transformed from triaxial into essentially oblate systems, with well-aligned isopotential contours of roughly constant flattening ($\langle c/a\rangle \sim 0.85$). Halos always contract as a result of galaxy assembly, but the effect is substantially less pronounced than predicted by the traditional "adiabatic contraction" hypothesis. The reduced contraction helps to reconcile ΛCDM halos with constraints on the dark matter content inside the solar circle and should alleviate the long-standing difficulty of matching simultaneously the scaling properties of galaxy disks and the galaxy luminosity function. The halo contraction we report is also less pronounced than found in earlier simulations, a disagreement that suggests that halo contraction is not solely a function of the initial and final distribution of baryons. Not only *how much* baryonic mass has been deposited at the center of a halo matters, but also the *mode* of its deposition. It might prove impossible to predict the halo response to galaxy formation without a detailed understanding of a galaxy's detailed assembly history.

Key words: Galaxy: disk – Galaxy: formation – Galaxy: kinematics and dynamics – Galaxy: structure

1 INTRODUCTION

Over the past couple of decades, cosmological N-body simulations have established a number of important results regarding the structure of cold dark matter (CDM) halos. In particular, broad consensus holds regarding the overall shape of the halo mass distribution and its radial mass profile. CDM halos are distinctly triaxial systems supported by anisotropic velocity dispersion tensors (Frenk et al., 1988; Jing & Suto, 2002; Allgood et al., 2006; Hayashi et al., 2007; Bett et al., 2007), a result that reflects the highly aspherical nature of gravitationally-amplified density fluctuations as they become non linear and assemble into individual halos. Despite their chaotic assembly, the spherically-averaged mass profile of CDM halos is nearly "universal", and can be approximated fairly accurately, regardless of halo mass or redshift, by scaling a simple formula (see, e.g., Navarro et al., 1996b, 1997, 2004, 2008).

One major limitation is that these results have been obtained from simulations that neglect the presence of the baryonic, luminous component of galaxy systems. Although this may be a suitable approximation in extremely dark matter-dominated systems, it is expected to fail in regions where baryons contribute a substantial fraction of the mass, as is the case in the luminous regions of normal galaxies like the Milky Way. The response of the dark halo to the

assembly of a galaxy is thus a crucial ingredient of models that attempt to interpret observational constraints in terms of the prevailing CDM paradigm.

There has been extensive work, both numerical and analytical, on the modification of the mass profile of a dark halo induced by the assembly of a central galaxy. Early results suggested that simple analytical prescriptions based on the conservation of adiabatic invariants gave an accurate description of the halo response. Following the early work by Barnes & White (1984), Blumenthal et al. (1986) devised a simple formula to link the dark mass profiles before and after the assembly of a galaxy. Given the initial, spherically-symmetric enclosed mass profiles of the dark matter, $M^i_{\rm dm}(r)$, and baryons, $M^i_b(r)$, one may derive the final dark mass profile, $M^f_{\rm dm}(r)$, once the final baryonic mass profile, $M^f_b(r)$, is specified. The model assumes that dark matter particles move on circular orbits before and after the contraction, and that their initial, r_i, and final, r_f, radii are related by the condition:

$$r_f\,[M^f_b(r_f) + M_{\rm dm}] = r_i\,[M_{\rm dm} + M^i_b(r_i)], \qquad (1)$$

where $M_{\rm dm} = M_{\rm dm}(r_f) = M_{\rm dm}(r_i)$ is the dark mass enclosed by each dark matter particle (i.e., no shell crossing).

Despite its simplicity, and the crude approximation on which it is based, early N-body work (e.g., Barnes & White, 1984; Blumenthal et al., 1986; Jesseit et al., 2002) found reasonable agreement between eq. 1 and the results of simulations, and helped to establish the "adiabatic contraction" formulation as the default procedure when considering the halo response to the formation of a central galaxy.

Semianalytic models of galaxy formation have adopted this formulation in order to link the (observed) dynamical properties of luminous galaxies to the (predicted) properties of the dark halos that surround them (see, e.g., Mo et al., 1998; Cole et al., 2000; Dutton et al., 2005; Croton et al., 2006; Somerville et al., 2008). This work has highlighted a number of potential problems when attempting to reconcile the predicted properties of galaxies in the ΛCDM cosmogony with observed scaling relations.

One particularly important challenge has been the inability of semianalytic galaxy formation models to match simultaneously the zero point of the Tully-Fisher (TF) relation and the galaxy luminosity function. Successful models require that the rotation speed of disks be of the order of the virial velocity of the halos they inhabit (see, e.g., Somerville & Primack, 1999; Croton et al., 2006). However, models that include adiabatic contraction typically predict disk rotation speeds well in excess of the virial velocity.

As discussed most recently by, for example, Dutton et al. (2005); Gnedin et al. (2007) and Dutton et al. (2008), potential solutions to this problem include: (i) revising the adiabatic hypothesis so as to reduce (or even reverse!) the halo contraction; (ii) adopting lighter stellar mass-to-light ratios in order to minimize the contribution of baryons and to allow for more dark mass enclosed within disk galaxies; or (iii) modifying the cosmological parameters so as to reduce halo concentrations. We shall concentrate our analysis here on option (i), although we note that all three possibilities are probably equally important and should be treated on equal footing when addressing these issues in semianalytic models of galaxy formation.

The possibility that the actual response of the halo to the assembly of the disk might differ substantially from the predictions of the adiabatic contraction formalism has been noted before. Barnes (1987) and Sellwood (1999) have remarked that the adiabatic contraction hypothesis might lead to substantial overestimation of the halo compression. As discussed by Sellwood & McGaugh (2005) and Choi et al. (2006), such deviations are likely to depend strongly on the orbital structure of a halo, performing best when most particles have large tangential motions, but poorly in systems with radially anisotropic velocity distributions.

It should also be pointed out that the studies mentioned above were carried out by perturbing simple spherical models with a potential term designed to imitate the growth of an assembling galaxy. These studies, therefore, miss the hierarchical nature of the assembly of a galaxy and of its surrounding halo. The study of Gnedin et al. (2004), on the other hand, uses the proper cosmological context, but focusses on simulations of galaxy clusters, rather than the galaxy-sized systems of interest for the issues discussed above. In this respect, our study is similar to that of Gustafsson et al. (2006), who studied four simulations of galaxy-sized halos in the ΛCDM scenario.

The assembly of a central galaxy also modifies the three-dimensional shape of the surrounding dark matter halo. This was already noted in the first simulations to include, in addition to a dark matter halo, a dissipative baryonic component, such as the early work of Katz & Gunn (1991) and Katz & White (1993). Dubinski (1994) studied this further by growing adiabatically a central mass concentration inside a triaxial dark matter halo and confirmed that the steepening of the potential leads to much rounder halo shapes. This result was confirmed by Kazantzidis et al (2004), who also noticed the effect in their cluster simulations. We extend this body of work by focussing, as in Hayashi et al. (2007), on the shape of the gravitational potential rather than on the axial ratios of the inertia tensor, as well as on its dependence on radius.

The plan of this paper is as follows: § 2 describes the numerical simulations and § 3 presents the main results. After a brief general description of the evolution in § 3.1, § 3.2 describes the main properties of the simulated central galaxies; § 3.3 discusses the modifications they induce on the shape of the halo gravitational potential; while § 3.4 compares the mass profiles of dark halos before and after the inclusion of a dissipative baryonic component. We apply these results to the Milky Way in § 3.5 and compare with earlier work in § 3.6. We end with a brief summary of our main conclusions in § 4.

2 NUMERICAL SIMULATIONS

2.1 Cosmological parameters

We adopt cosmological parameters consistent with the combined analysis of the 2dfGRS (Colless et al., 2001) and the first-year WMAP data (Spergel et al., 2003): a present day value of the Hubble constant of $H_0 = 70$ km/s/Mpc; a scale-free initial density perturbation spectrum with no tilt and normalized by the linear rms mass fluctuations on $8h^{-1}$ Mpc spheres, $\sigma_8 = 0.9$. The matter-energy content of the Universe is expressed in units of the present-day critical

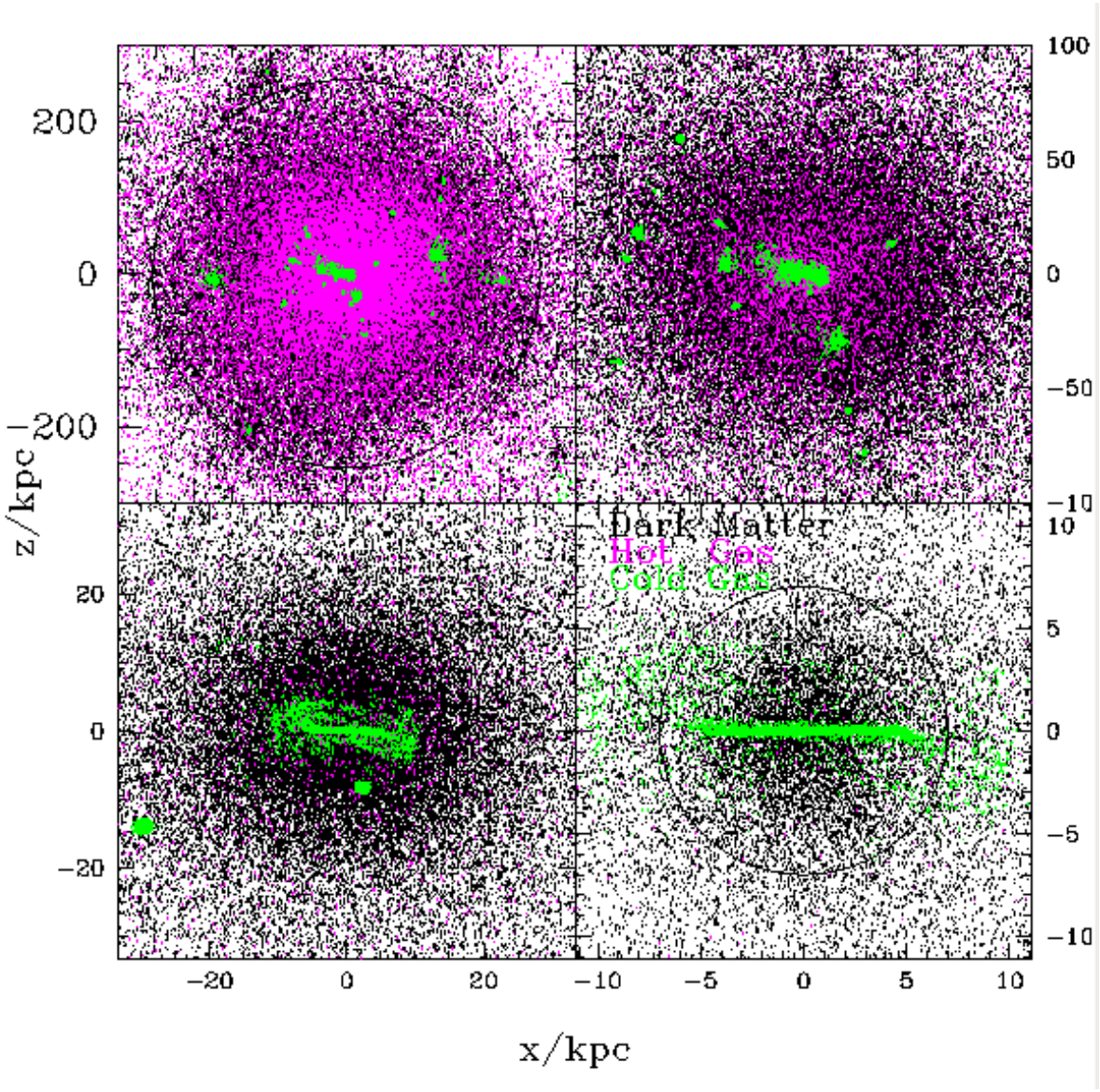

Figure 1. Dark matter (black) and gas (colored) particles for halo S02h. The color of a gas particle reflects its temperature, $T < 10^{4.5}$K (green) or $T > 10^{4.5}$K (magenta). Each panel zooms into the center of the system by consecutive factors of 3 in radius (see axis labels). The circle in the top-left panel shows the virial radius. The circle in the bottom-right panel shows the radius, $r_{\rm glx}$, used to define the central galaxy. Note that the colder (green) gas component inhabits the center of the main halo and of its substructures, where it forms thin, centrifugally-supported disks. The hotter component (magenta) is distributed more or less uniformly across the main halo and makes up only 16% of all the baryons within the virial radius.

density for closure, and contains a dominant cosmological constant term, $\Omega_\Lambda = 0.7$, as well as contributions to the matter content, $\Omega_{\rm M} = 0.3$, from cold dark matter (CDM), $\Omega_{\rm CDM} = 0.259$, and baryons, $\Omega_{\rm b} = 0.041$.

2.2 Code and initial conditions

We have performed a suite of 13 numerical simulations of the formation of galaxy-sized halos in the ΛCDM cosmogony. Each simulation follows the evolution of a relatively small region of the Universe, excised from a 432^3-particle simulation of a large $50\,h^{-1}$ Mpc periodic box (Reed et al., 2003), and resimulated at much higher mass and spatial resolution. Each "zoomed-in" re-simulation follows the formation of a single galaxy-sized halo of mass $\sim 10^{12}\,M_\odot$ and its immediate surroundings. The simulations include the tidal fields of the parent simulation, and follows the coupled evolution of gas and dark matter. The hydrodynamical evolution of the gaseous component is followed using the Smooth Particle Hydrodynamics (SPH) technique. This re-simulation technique follows standard practice, as described, for example, by Power et al. (2003). All our simulations were performed using GASOLINE, a parallel N-body/SPH code described in detail by Wadsley et al. (2004).

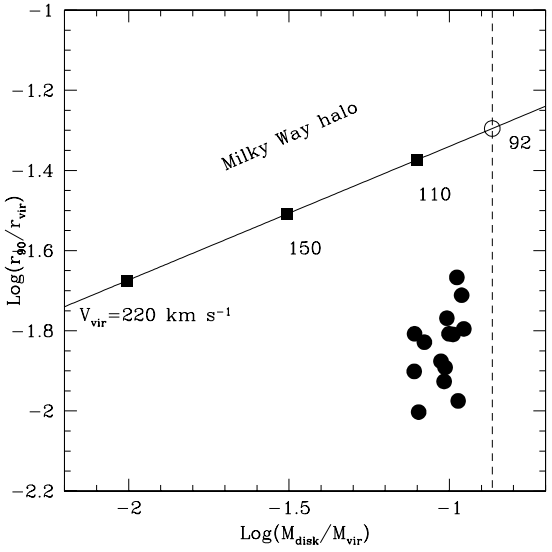

Figure 2. Radius containing 90% of the baryonic mass, r_{90}, versus the total baryonic mass of the central galaxy, $M_{\rm disk}$, in our simulated halos (filled circles), expressed in units of the halo virial values. The dashed vertical line the universal baryon fraction, $f_{\rm bar} = \Omega_b/\Omega_{\rm M}$. About 70-80% of all baryons have been collected in the central galaxy. The solid curve shows the corresponding values for the Milky Way, varying the virial mass of its halo. Symbols along the line indicate a few different values of the virial velocity, $V_{\rm vir}$ = 220, 150, 110, and 91 km/s. Note that the simulated central galaxies are substantially more massive and smaller than spirals like the Milky Way. This maximizes the effect of baryons in transforming the shape and mass profile of the dark halo.

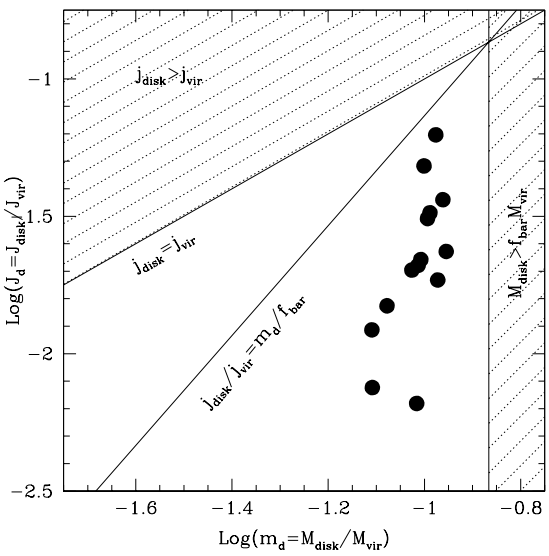

Figure 3. Angular momentum and mass of the central galaxy in our simulations, expressed in units of the virial values. The curve labeled $j_{\rm disk} = j_{\rm vir}$ corresponds to central galaxies with the same *specific* angular momentum as the surrounding halo (a common assumption of semianalytic models). Those on the curve labeled $j_{\rm disk}/j_{\rm vir} = m_d/f_{\rm bar}$ have specific angular momenta (in units of the halo's) that scale in proportion to the fraction of baryons within the virial radius that have collected in the central galaxy. Note that the simulated central galaxies have even lower angular momenta than in the latter assumption, highlighting the large angular momentum losses that accompany the assembly of the central galaxy, and explaining the small sizes of the disks shown in Fig. 2.

2.3 Halo selection and resimulation

The 13 halos were selected from a list of all $\sim 10^{12}\,M_\odot$ halos in the parent simulation, with a mild bias to avoid objects that have undergone a major merger after $z = 1$ or that have, at $z = 0$, unusually low ($\lambda < 0.03$) spin parameter. The mass resolution of the resimulations is such that halos are represented with $\sim 40,000$ dark matter particles within their virial radius * at $z = 0$. Two sets of simulations are performed for each halo, one where only a dark matter component is followed, and another where dark matter and baryons are included. Dark matter-only simulations ("DMO" for short) assume that the total matter content of the Universe is in cold dark matter, $\Omega_{\rm M} = \Omega_{\rm CDM} = 0.3$.

Simulations including a baryonic component ("DM+B" for short) include equal number of gas and dark matter particles, with masses modified to satisfy our choice of $\Omega_b = 0.041$ and $\Omega_{\rm CDM} = 0.259$. The gaseous component is evolved using SPH including, besides the self-gravity of gas and dark matter, pressure gradients and shocks. Baryons are allowed to cool radiatively according to the cooling function of a gas of primordial composition down to a temperature of 10^4 K, below which cooling is disabled. No star formation or feedback is included. As we discuss below, this choice maximizes cooling and favors the collection of most baryons at the center of each dark halo. Although unrealistic as a model for galaxy formation, this choice has the virtue of simplicity and also allows us to examine the halo response when the effect of the baryonic component is maximal.

Pairwise gravitational interactions are softened adopting a spline softening length kept fixed in comoving coordinates. We test for numerical resolution effects by simulating each halo with 8 times fewer particles. In the interest of brevity we do not present results from this low-resolution series here, but we have checked explicitly that none of the conclusions we present here are modified by this change in numerical resolution. We have also increased the number of particles in one case. Halo S02h is equivalent to S02, but with $\sim$ 3.4 times more particles: at $z = 0$ this halo has $\sim 140,000$ particles per component within the virial radius.

Table 1 lists the main properties of the simulated halos.

* We define the *virial* radius, $r_{\rm vir}$, of a system as the radius of a sphere of mean density $\Delta_{\rm vir}(z)$ times the critical density for closure. This definition defines implicitly the virial mass, $M_{\rm vir}$, as that enclosed within $r_{\rm vir}$, and the virial velocity, $V_{\rm vir}$, as the circular velocity measured at $r_{\rm vir}$. Quantities characterizing a system will be measured within $r_{\rm vir}$, unless otherwise specified. The virial density contrast, $\Delta_{\rm vir}(z)$ is given by $\Delta_{\rm vir}(z) = 18\pi^2 + 82f(z) - 39f(z)^2$, where $f(z) = [\Omega_0(1+z)^3/(\Omega_0(1+z)^3 + \Omega_\Lambda))] - 1$ and $\Omega_0 = \Omega_{\rm CDM} + \Omega_b$(Bryan & Norman, 1998). $\Delta_{\rm vir} \approx 100$ at $z = 0$.

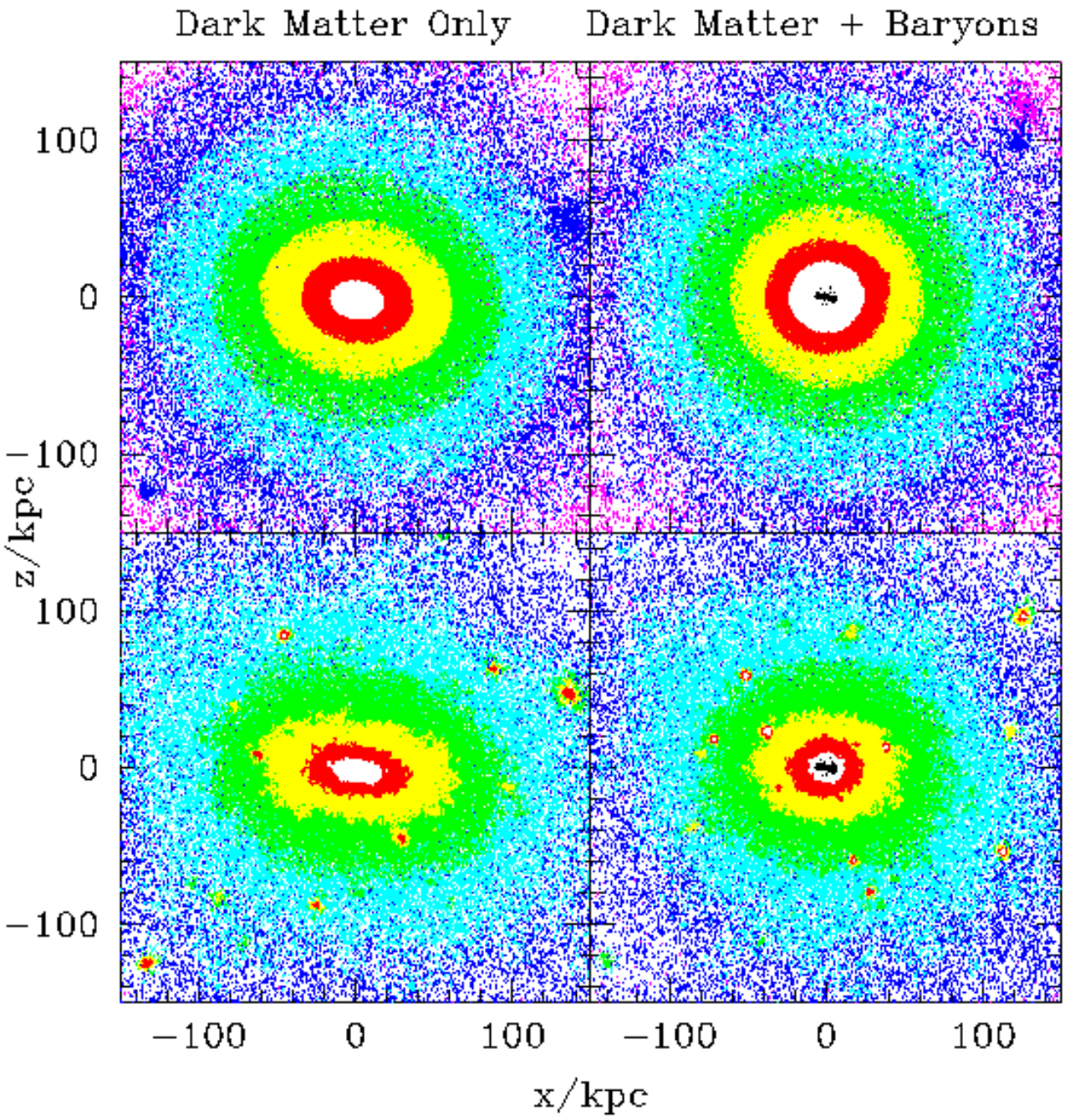

Figure 4. Dark matter particles corresponding, at $z = 0$, to the two resimulations of halo S02h, "dark matter only" (left panels) and "dark matter plus baryons" (right panels). Particles are colored according to the value of the gravitational potential (binned in logarithmic units, top panels) or the local density (bottom panels). Note that the halo responds to the assembly of the central galaxy (shown in black in the right-hand panels) by becoming noticeably more spherical. Projections are chosen so that the rotation axis of the central disk coincides with the z-axis. The central disk is shown with black dots, to illustrate the orientation of the disk relative to the halo shape. In general, the central disk is well aligned with the minor axis of the halo.

3 RESULTS

3.1 General evolution

Because our simulations neglect the formation of stars and their feedback, the evolution of the baryonic component is characterized by the rapid cooling and collapse of baryons at the center of the early collapsing progenitors of the final halo. As a result, the main mode of galaxy assembly is mergers: up to 70% of all baryons in the central galaxy were accreted in the form of dense, cold, gaseous clumps that sink to the center through dynamical friction.

As shown in earlier work, (see, e.g., Navarro & Benz,

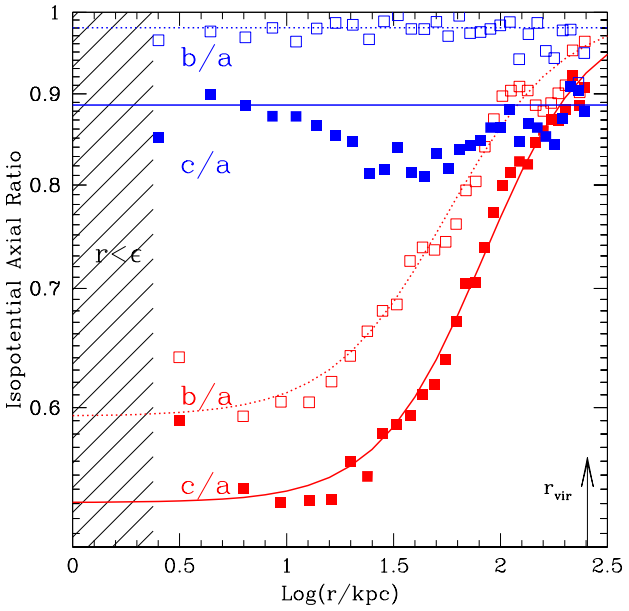

Figure 5. "Radial" ($r = \sqrt{a^2+b^2+c^2}$) dependence of axial ratios b/a (open symbols) and c/a (filled symbols) for our high-resolution run S02h. Halo shapes are measured by fitting 3D ellipsoids to the position of dark matter particles in narrow logarithmic bins of the gravitational potential. The potential is computed using *only* dark matter particles, so it actually corresponds to the contribution of the dark matter component to the overall potential. Red (lower) symbols correspond to the DMO run; blue (upper) symbols to the DM+B run. Note that the central galaxy turns a rather triaxial, nearly prolate halo into an axisymmetric, nearly oblate one. Curves are fits using eq. 2. Fit parameters for this halo and the mean value computed over the sample are listed in Table 2.

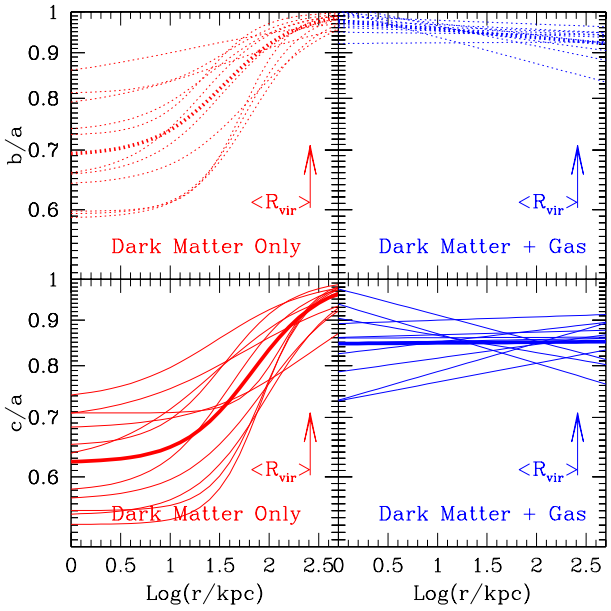

Figure 6. "Radial" ($r = \sqrt{a^2+b^2+c^2}$) dependence of axial ratios b/a (upper panel) and c/a (lower panel) for all simulated haloes. The curves for the "dark matter only" runs are computed by fitting eq. 2 to the radial dependence of the axial ratios of particles along isopotential contours. The contours in all cases refer to the potential contributed solely by the dark matter component. Note that, as a result of the assembly of the central galaxy, (i) halos become nearly oblate and (ii) axial ratios become approximately independent of radius. The effect on the shape of the halo extends almost to the virial radius, far beyond the actual size of the central galaxy. Thick lines correspond to mean values computed over the sample.

1991; Navarro & White, 1994; Navarro et al., 1997), this mode of assembly leads to very efficient accretion of baryons into the central galaxy and to the transfer of much of their angular momentum to the surrounding halo. Because baryons are assumed to remain in gaseous form at all times, those that can cool are forced to settle into centrifugally-supported disks at the center of their surrounding dark halos. Thus, we expect the central galaxies in our simulations to be disks that contain a large fraction of all baryons within the virial radius, and to have angular momenta well below the angular momentum content of the system as a whole.

Figure 1 illustrates this for the case of our highest resolution halo, S02h (see Table 1). The four panels in this figure show the dark matter (black) and baryonic (colored) components, zooming by consecutive factors of 3 toward the central galaxy. Cold gas ($T < 10^{4.5}$K) is shown in green, whereas hot gas ($T > 10^{4.5}$K) is shown in magenta. Note that most of the cold gas inhabits the center of the main halo and its substructures, where it forms easily identifiable thin, massive disks. All cold baryons associated with the central disk are contained within a sphere of radius $r_{\rm glx} = 10$ kpc, which we shall use hereafter to define the central galaxy in all runs.

3.2 Mass, size and angular momentum of central galaxies

The central galaxy contains most of the baryons within the virial radius of the system (74% in the case of S02h, see Table 1). This is shown in Fig. 2, where we plot, for all our simulations, the baryonic mass of the central galaxy, $M_{\rm disk}$, versus the radius, r_{90}, that contains 90% of its mass, scaled to the virial mass and radius of the system, respectively. The vertical dashed line indicates the universal baryon fraction in the simulations, $f_{\rm bar} = \Omega_{\rm bar}/\Omega_{\rm M} = 0.137$. Typically, 70 to 80% of all baryons within $r_{\rm vir}$ are found in fairly small central disks that are fully contained within a radius of order $\sim 3\%$ of the virial radius.

We may compare this with a typical spiral galaxy like the Milky Way (MW), where the mass and size of the baryonic component can be estimated accurately. Assuming that the disk is exponential with total mass $4.5 \times 10^{10}\,M_\odot$ and radial scalelength $R_d^{\rm MW} = 2.5$ kpc and that the mass of the bulge is $M_{\rm bulge} = 4.5 \times 10^9\,M_\odot$, we estimate that 90% of the Milky Way baryons are confined within $r_{90}^{\rm MW} = 9.4$ kpc.

In order to compare this with the simulation results shown in Fig. 2 we need make an assumption about the virial mass of the Milky Way halo. For a virial velocity of the order of the rotation speed at the solar circle (220 km/s), the baryonic component makes up only $\sim 1\%$ of the virial mass, or roughly 7% of all baryons within $r_{\rm vir}$. The simulated

disks are thus much smaller than a typical spiral like the MW. They are also comparatively more massive.

Only if the virial velocity is as low as 110 km/s do the MW bulge+disk make up a fraction of available baryons as high as in our simulations ($\sim$ 75%). However, in that case $r_{90}^{\rm MW} \sim 0.06 r_{\rm vir}$, a factor of ~ 4 times larger than our simulated disks.

The reason why simulated gaseous disks are so much smaller than typical spirals is that baryons have lost a large fraction of their angular momentum to the surrounding halo. This is illustrated in Fig 3. where we plot the angular momentum of the gaseous disk (in units of that of the system as a whole, which is dominated by the dark matter component), $J_d \equiv J_{\rm disk}/J_{\rm vir} = M_{\rm disk}\, j_{\rm disk}/M_{\rm vir}\, j_{\rm vir}$, versus the mass fraction, $m_d \equiv M_{\rm disk}/M_{\rm vir}$. These are the parameters commonly adopted in semianalytic models of disk formation, such as those of Mo et al. (1998).

Since baryons acquire during the expansion phase as much angular momentum as the dark matter, and it is unlikely that $M_{\rm disk}/M_{\rm vir}$ will exceed the universal baryon fraction, then we do not expect the *specific* angular momentum of the disk, $j_{\rm disk}$, to exceed that of the system as a whole, $j_{\rm vir}$. Therefore, central galaxies are unlikely to populate the shaded areas of Fig. 3.

Most semianalytic work assumes, for simplicity, that $j_{\rm disk} = j_{\rm vir}$ or, equivalently, that $J_d = m_d$, regardless of the value of m_d. On the other hand, Navarro & Steinmetz (2000) argue that it is unlikely that a galaxy where $m_d << f_{\rm bar}$ may have the same specific angular momentum as the whole system, and propose that $j_{\rm disk}$, as a fraction of $j_{\rm vir}$, should be comparable to the fraction of baryons that make up the central galaxy; i.e., $j_{\rm disk}/j_{\rm vir} = M_{\rm disk}/(f_{\rm bar} M_{\rm vir}) = m_d/f_{\rm bar}$. This is illustrated in Fig. 3 by the lower diagonal line.

Our simulated galaxies are well below both lines. This indicates that baryons have specific angular momenta much lower than their surrounding halos and explains their small sizes compared to typical spirals. These are therefore unrealistic models of spiral galaxy formation, but the combination of large mass and small size allows us to probe the response of the dark halo in the case where the deepening of the potential well due to the central galaxy is maximal.

3.3 Halo shape

As anticipated in § 1, the halo responds to the presence of the central galaxy by becoming significantly more spherical. This is illustrated in Fig. 4, where we compare the shape of isodensity and isopotential contours for the "dark matter only" and "dark matter plus baryons" runs of halo S02h. Panels on the left correspond to the DMO run, those on the right to the DM+B run. Particles are colored according to their local values of their gravitational potential or local density (binned in a logarithmic scale), computed using *only* the dark matter particles. Note that using the gravitational potential leads to much more stable estimates of the shape of the halo, since it is much less affected by the presence of substructures and other transient fluctuations in the mass distribution.

The isopotential contours are well approximated by ellipsoidal surfaces, and we use the axial ratios of such ellipsoids to measure, as a function or radius, the change in shape of halo S02h. We show the result in Fig. 5. As discussed by Hayashi et al. (2007), the radial dependence of the axial ratios may be approximated by the formula,

$$\log(\frac{b}{a} \text{ or } \frac{c}{a}) = \alpha \left[\tanh\left(\gamma \log \frac{r}{r_\alpha}\right) - 1\right], \quad (2)$$

Here α parameterizes the central value of the axial ratio, $(b/a)_0$ or $(c/a)_0$, by $10^{-2\ \alpha}$; r_α indicates the characteristic radius at which the axial ratio increases significantly from its central value; and γ regulates the sharpness of the transition.

The presence of the central galaxy turns the halo from a triaxial, nearly prolate system into an axisymmetric, nearly oblate system where the axial ratio is nearly constant with radius. As a result, eq. 2 is not adequate for the nearly featureless radial dependence of the axial ratios in the DM+B runs. We fit the latter with a simple power-law,

$$\log(\frac{b}{a} \text{ or } \frac{c}{a}) = \alpha \log r + \beta, \quad (3)$$

The best-fit parameter to the mass and isopotential contour profile shapes are given in Table 2.

The profile fits for all simulations are compiled in Fig. 6, and illustrate a few important points. As a result of the assembly of the central galaxy: (i) halos become nearly oblate; (ii) axial ratios are roughly independent of radius; and (iii) halo shapes are affected well beyond the size of the central galaxy, and nearly as far out as the virial radius.

3.4 Mass profile and contraction

Fig. 7 shows the enclosed mass profile of the DMO and DM+B runs corresponding to halo S02h. DMO dark masses have been scaled by $(1 - f_{\rm bar})$ so that the total dark mass in both the DMO and DM+B runs are the same. The DMO mass profile is shown by the thick red solid curve and, as expected, it is well approximated by the NFW (Navarro et al., 1996b, 1997) formula (thin solid line). The central disk that assembles in the DM+B run leads to a contraction of the dark halo: there is *more* dark mass in the DM+B run *at all radii* compared with the DMO run. This is a result common to all our simulations; in no case do we see the halo "expand" as a results of the assembly of the central galaxy.

The contraction, however, is not as pronounced as what would be expected from the "adiabatic contraction" model discussed in § 1. The adiabatic contraction prediction (eq. 1) is shown by the thick dotted line in Fig. 7. The discrepancy between model and numerical results is not small. At $\sim$ 5 kpc, a radius roughly twice the gravitational softening and that encloses more than 1300 dark particles, the adiabatic-contraction formula predicts $\sim$ 2.5 *times more dark mass than found in our simulations*. Even at a radius of 10 kpc, eq. 1 overestimates the halo contraction by more than $\sim$ 50% in mass. The modified contraction proposed by Gnedin et al. (2004) (see curve labeled "Contra" in Fig. 7) fares better, but it still overpredicts the results of the simulations.

A similar result applies to all of our simulated halos. We illustrate this in Fig. 8, where we plot the ratio between radii that contain a given number of dark matter particles in the DMO run (r_i) and the DM+B run (r_f) versus the ratio between M_i, the total mass within r_i in the DMO run, and M_f, the total mass within r_f in the DM+B run. With this choice, the adiabatic-contraction prediction is simply $r_f/r_i = M_i/M_f$, which is traced by the 1:1 line in Fig. 8.

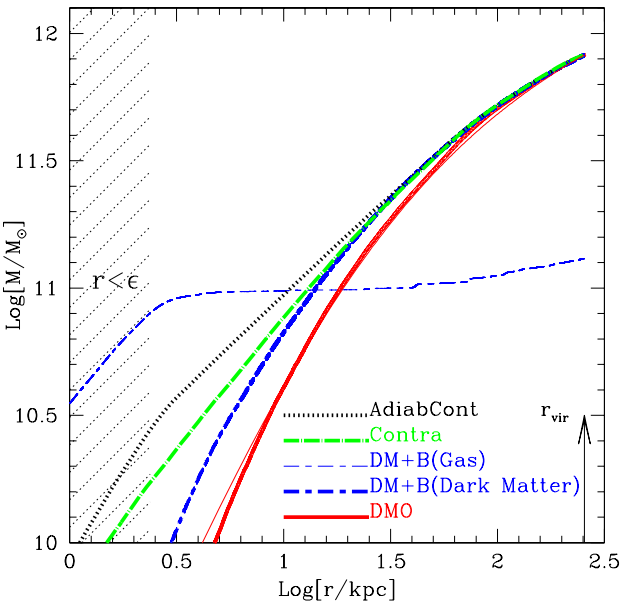

Figure 7. Enclosed mass profile of various components of halo S02h. The "dark matter only" profile is shown with a thick curve, after scaling masses by $(1 - f_{\rm bar})$, so that, within $r_{\rm vir}$, the total dark mass of the DMO and DM+B runs will be comparable. The thin line shows a Navarro-Frenk-White halo fit to the DMO profile. Other colors and line types correspond to the various components of the DM+B run, as specified in the figure labels. The thick dashed blue curve shows the dark mass profile for the DM+B run. The assembly of most baryons into a central galaxy (dotted magenta curve) has clearly led to a contraction of the dark mass profile. The profile predicted by the "adiabatic contraction" formula (eq. 1; dot-dashed green curve) overpredicts the response of the halo. The modified adiabatic contraction model of Gnedin et al. (2004), shown by the dotted cyan curve, also overestimates the halo response.

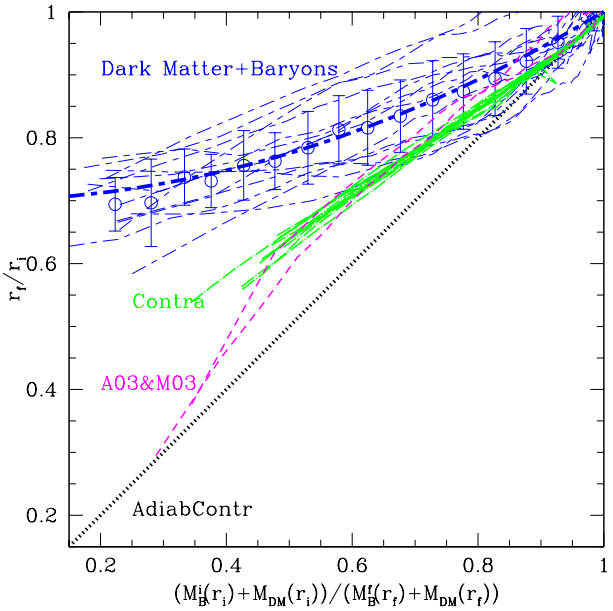

Figure 8. Dark halo response to the assembly of a central galaxy. The ordinate shows the ratio, r_f/r_i, between the radius containing a given amount of dark mass in the DMO and DM+B runs, respectively, after scaling DMO masses by $1 - f_{\rm bar}$. The smaller r_f/r_i the stronger the halo contraction. The x-axis shows the ratio between the total mass, M_i, contained within r_i (in the DMO run) and M_f, that enclosed within r_f (in the DM+B run). The adiabatic contraction formula (eq. 1) predicts that $r_f/r_i = M_i/M_f$; this is shown by the 1:1 line in the figure. Numerical results are shown for individual halos; from the radius that contains 1000 dark particles outwards in order to minimize numerical uncertainties. The adiabatic-contraction formula overestimates the halo response. Gnedin et al. (2004)'s modified adiabatic contraction ("Contra") does better but still overpredicts the halo response at most radii, and especially near the center. Symbols with error bars trace the median and quartiles of the numerical results. The thick upper curve is a fit using eq. 4.

The numerical simulations are shown by the upper curves in this figure. Near the center, the baryons dominate over the DMO mass profile, and therefore $M_i/M_f \ll 1$. Further out, the contribution of baryons to the total enclosed mass decreases, approaching the universal baryon fraction at the virial radius, where M_i/M_f tends to unity. The innermost radius plotted in each case corresponds to that enclosing 1000 dark matter particles. This is in all cases comfortably larger than the gravitational softening, minimizing the possibility that our results are unduly influenced by numerical artifact. The open circles with error bars in Fig. 8 trace the median and rms scatter of all our simulation results.

The ratio r_f/r_i tends to a constant for $M_i/M_f \ll 1$, suggesting that the halo response approaches saturation in regions where baryons dominate. A simple formula captures the average behaviour well (thick upper solid line),

$$r_f/r_i = 1 + a[(M_i/M_f)^n - 1], \qquad (4)$$

with $a = 0.3$ and $n = 2$. As an application, we shall use this expression below to explore what constraints this implies for the mass and concentration of the halo of the Milky Way.

3.5 Application to the Milky Way

The Milky Way offers a case study for the results described above. Because the mass and radial distribution of the baryonic component, as well as the rotation speed of the local standard of rest (LSR), are relatively well known, the total dark mass contained within the solar circle is firmly constrained. Adopting the same quantities for the bulge and disk of the Milky Way adopted in § 3.2, we find that baryons contribute (in quadrature) ~ 171 km/s to the circular velocity of the LSR, which we assume to be 220 km/s. This implies that the dark mass of the Milky Way within the solar circle ($R_\odot = 8$ kpc) is $\sim 3.5 \times 10^{10}\, M_\odot$. In order to allow for the possibility that some of this dark mass may be baryonic, we shall treat this a formal upper limit in the analysis that follows.

The second constraint comes from the total baryonic mass of the Milky Way, under the plausible assumption that the mass of the central galaxy cannot exceed the total mass of baryons within the virial radius, $\approx f_{\rm bar} M_{\rm vir}$. Thus, the *minimum* virial mass allowed for the MW halo by this con-

straint is $3.64 \times 10^{11}\, M_\odot$, which corresponds to a virial velocity of ~ 92 km/s.

Are these constraints compatible with ΛCDM halos? The top left panel of Fig. 9 shows the dark mass expected within 8 kpc vs halo virial velocity. Each dot in this panel correspond to an NFW halo with concentration drawn at random from the mass-concentration relation (including scatter) derived by Neto et al. (2007) from the Millennium Simulation (Springel et al., 2005). As expected, the mass within 8 kpc increases with the virial velocity (mass) of the halo, modulated by the fairly large scatter in concentration at given halo mass.

The black "wedge" in this panel indicates the region allowed by the MW constraints discussed above. As discussed by Eke et al. (2001), most ΛCDM halos satisfy the constraints, and would be consistent with the MW if they were somehow able to avoid contraction. Note as well that the larger the MW halo virial velocity the lower the allowed concentration. For $V_{\rm vir} = 220$ km/s (the value required by semi-analytic models to match the Tully-Fisher relation and the luminosity function, see § 1) only halos with $c_{\rm vir} < 9.5$ would be consistent with the Milky Way. For comparison, the average concentration of $V_{\rm vir} = 220$ km/s halos is $\langle c_{\rm vir}\rangle \sim 10.4$ and its (lognormal) dispersion is $\sigma_{\log c} = 2.9$, so this condition effectively excludes only 57% of such halos from the allowed pool.

The situation is rather different if halos are adiabatically contracted (panel labeled "AdiabCont" in Fig. 9). The contraction increases substantially the dark mass contained within 8 kpc, so that very few halos satisfy the MW constraints. For example, essentially no halo with $V_{\rm vir} \approx 220$ km/s could host a galaxy like the Milky Way, and the few that could would need to have $c_{\rm vir} < 3.2$, many sigma away from the average concentration of halos of that mass. The halo of the Milky Way would need to be a very special halo of unusually low concentration if adiabatic contraction holds.

Adopting the halo contraction of our numerical simulations improves matters. This may be seen in the bottom-left panel of Fig. 9, where we have contracted each halo using eq. 4. The range of allowed halo masses and concentrations is broader; even some halos with $V_{\rm vir} \sim 220$ km/s could be consistent with the Milky Way, provided that $c_{\rm vir} < 6.5$. This is significantly lower than the average at that mass, but conditions are much less restrictive if the halo of the Milky Way is less massive; for example, half of all $V_{\rm vir} \sim 130$ km/s halos satisfy the MW constraints. The possibility that the virial velocity of the Milky Way is significantly lower than 220 km/s has indeed been advocated by a number of recent observational studies (Smith et al., 2007; Sales et al., 2007; Xue et al., 2008).

Lowering the average concentration at given mass also helps. This is shown in the bottom-right panel of Fig. 9, where we have repeated the exercise, but lowering all concentrations by 20%. According to Duffy et al. (2008), this is approximately the change in average concentration when modifying the cosmological parameters from the values we adopt here (which are consistent with the first-year analysis of the WMAP satellite data) to those favoured by the latest 5-year WMAP data analysis. With this revision, 18% of $V_{\rm vir} \sim 220$ km/s halos and roughly half of all $V_{\rm vir} \sim 160$ km/s halos would be consistent with the MW.

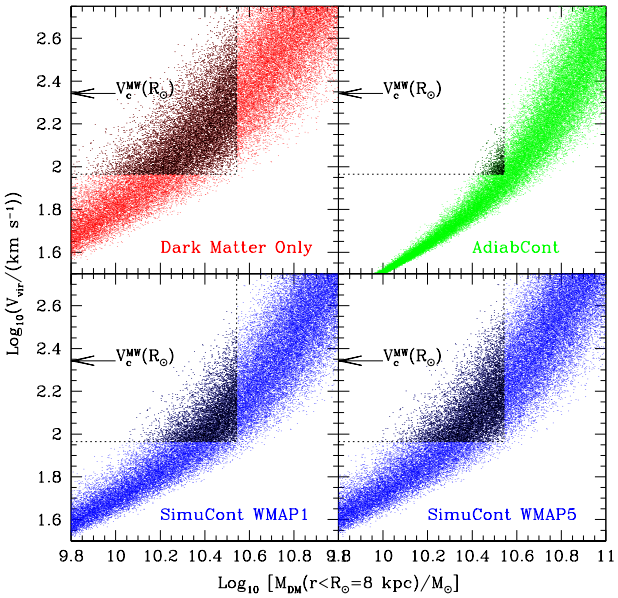

Figure 9. Dark mass within 8 kpc vs virial velocity for halos drawn at random from the ΛCDM mass-concentration relation (including scatter) of Neto et al. (2007). The DMO panel (top left) shows the results neglecting the effects of baryons and assuming an NFW profile for the dark halos. The black "wedge" highlights the region of parameter space compatible with observations of the Milky Way. The panel labeled "AdiabCont" shows the result of contracting each halo adopting the adiabatic contraction formula (eq. 1). Very few halos would be consistent with the Milky Way if this formula holds. The bottom-left panels shows the result of applying our simulation results for the halo contraction, as captured by eq. 4. The bottom-right panel repeats the same exercise, but after reducing all concentrations by 20% in order to mimic the expected concentration change resulting from adopting the latest cosmological parameters from the 5-year analysis of WMAP satellite data (Duffy et al., 2008).

3.6 Comparison with earlier work

The failure of the adiabatic contraction formalism to match the results of our simulations suggest that the response of the halo is more complex than what can be captured with a simple model for the contraction of spherical shells. This is confirmed by comparing our results with earlier work.

Our results disagree not only with the traditional adiabatic contraction formula, but also with the modified formalism proposed by Gnedin et al. (2004) (shown with thin dash-dotted green lines in Fig. 8). These authors calibrated their results with numerical simulations not dissimilar to ours, except for the mass scale—they used mainly galaxy cluster halos. The mass scale, on the other hand, does not seem to be the reason for the discrepancy. Our halo contraction is also less pronounced than found in two galaxy-sized halo simulations, as shown by the lines labeled A03&M03 in Fig. 8. These correspond to gasdynamical simulations of galaxy formation presented by Abadi et al. (2003a,b) and Meza et al. (2003), and differ from ours mainly in their inclusion of star formation and feedback effects. Those two

simulations seem to agree better with the "Contra" predictions than with our simulation results.

Barring numerical artifact, these results seem to suggest that *the halo response does not depend solely on the initial and final distribution of baryons*. One possible explanation is that not only *how much* baryonic mass has been deposited at the center of a halo matters, but also the *mode* of its deposition. It is certainly plausible that central galaxies assembled through merging of dense subclumps may lead to different halo response than galaxies assembled through a smooth flow of baryons to the center. Mergers of baryonic subsystems may in principle pump energy into the dark halo (through dynamical friction), altering its central structure and softening its contraction. This possibility has been argued before (see, e.g., El-Zant et al., 2001; Ma & Boylan-Kolchin, 2004; Mo & Mao, 2004), and seems to find favor in our simulations, where mergers between massive baryonic clumps are frequent and plentiful and halo contraction is less strong than reported in earlier work.

Recent work has also speculated that mergers may lead to halo *expansion* and that this would help to reconcile the properties of disk galaxies with ΛCDM halos (Dutton et al., 2007). Our halos always contract, and it seems safe to conclude that our results reflect the maximum effect of mergers on the halo response. We conclude therefore that mergers alone are unlikely to result in halo expansion. If such expansion is truly needed to reconcile disk properties with ΛCDM halos, it should come as a consequence of other processes not considered here, such as feedback-driven winds that may remove substantial fraction of baryons from the central galaxy (see, e.g., Navarro et al., 1996a; Babul & Ferguson, 1996).

4 SUMMARY

We have used a suite of cosmological N-body/gasdynamical simulations to examine the modifications to the dark halo structure that result from the assembly of a central galaxy. The formation of 13 ΛCDM halos is simulated twice, with and without a baryonic (gaseous) component. For simplicity, the gasdynamic simulations include radiative cooling but neglect star formation and feedback. This favors the formation of massive central baryonic disks at the center of the early collapsing progenitors of the final halo. As these systems merge, the gaseous clumps merge and re-form a disk at the center of the remnant.

The merger process leads to the transfer of a large fraction of the angular momentum from the baryons to the halo. At $z = 0$, the simulated central galaxies are too massive and too small to be consistent with observed spiral galaxies. Although unrealistic as a disk galaxy formation model, these simulations allow us to probe the dark halo response in the interesting case where the deepening of the potential well resulting from the formation of the central galaxy is maximized. Our main conclusions may be summarized as follows.

- Dark halos become significantly more spherical as a result of the assembly of the central galaxy. The triaxial, nearly prolate systems that form in the absence of a baryonic component are transformed into essentially oblate systems with a roughly constant axial isopotential ratio $\langle c/a \rangle \approx 0.85$.
- Halos always contract in response to the formation of the central galaxy. The "adiabatic contraction" formalism overestimates the halo contraction in our simulations. The discrepancy increases toward the centre, where the effect of baryons is larger. A simple empirical formula (eq. 4) describes our numerical results.
- The halo contraction in our simulations is also less pronounced than found in earlier numerical work (see, e.g., Gnedin et al., 2004), and suggest that the response of a halo does not depend on the final mass and radial distribution of baryons in the central galaxy, but also on the mode of their assembly.
- We apply these results to the Milky Way, where accurate estimates of the mass of baryons and dark matter inside the solar circle exist. These allow us to probe the range of halo virial mass and concentration consistent with the constraints. Only halos of unusually low mass and concentration would match such constraints if "adiabatic contraction" holds.
- This restriction is less severe if one uses the halo contraction reported here (eq. 4): although few ΛCDM halos of virial velocity ~ 220 km/s would be eligible hosts for the Milky Way, the situation improves for lower virial velocities. Halos of average concentration with virial velocity as large as $V_{\rm vir} = 135$ km/s, would be consistent with the MW constraints.

The dark halo response to the formation of a galaxy seems inextricably linked to the full coupled evolution of baryons and dark matter and may vary from system to system. Progress in our understanding of the distribution of dark matter in a baryon-dominated system will thus likely develop in step with our understanding of the particular assembly history of each individual system.

ACKNOWLEDGMENTS

We thank James Wadsley, Joachim Stadel and Tom Quinn for allowing us to use their excellent GASOLINE code for the numerical simulations reported here.

REFERENCES

Abadi M. G., Navarro J. F., Steinmetz M., Eke V. R., 2003a, ApJ, 591, 499
Abadi M. G., Navarro J. F., Steinmetz M., Eke V. R., 2003b, ApJ, 597, 21
Allgood B., Flores R. A., Primack J. R., et al., 2006, MNRAS, 367, 1781
Babul A., Ferguson H. C., 1996, ApJ, 458, 100
Barnes J., White S. D. M., 1984, MNRAS, 211, 753
Barnes J. E., 1987, in Nearly Normal Galaxies. From the Planck Time to the Present, edited by S. M. Faber, 154–159
Bett P., Eke V., Frenk C. S., Jenkins A., Helly J., Navarro J., 2007, MNRAS, 376, 215
Blumenthal G. R., Faber S. M., Flores R., Primack J. R., 1986, ApJ, 301, 27
Bryan G. L., Norman M. L., 1998, ApJ, 495, 80
Choi J.-H., Lu Y., Mo H. J., Weinberg M. D., 2006, MNRAS, 372, 1869
Cole S., Lacey C. G., Baugh C. M., Frenk C. S., 2000, MNRAS, 319, 168
Colless M., Dalton G., Maddox S., et al., 2001, MNRAS, 328, 1039

Label	$M_{\rm vir}$ $[10^{12}M_\odot]$	$r_{\rm vir}$ [kpc]	$N_{\rm DMO}$ $(<r_{\rm vir})$	N_{DM} $(<r_{\rm vir})$	$N_{\rm gas}$ $(<r_{\rm vir})$	$N_{\rm gas}$ $(<r_{\rm glx})$	$j_{\rm DMO}$ [kpc km s^{-1}]	$j_{\rm DM}$ [kpc km s^{-1}]	$j_{\rm gas}$ [kpc km s^{-1}]
S01	1.22	277.82	53009	52684	54732	38260	1847.7	2162.4	462.0
S02	0.94	254.18	40847	40687	39775	30613	1063.3	1088.3	332.8
S02h	0.95	255.89	139748	139729	140618	104309	1095.7	1200.3	359.1
S03	1.51	298.24	65729	65376	66416	37445	2593.9	2883.4	438.1
S04	0.85	246.02	37419	36432	39007	29534	1443.1	1626.7	508.8
S05	0.99	258.64	42564	42334	45270	30266	2505.0	2543.2	173.3
S06	1.22	278.05	53509	52652	55674	30411	2736.0	3056.0	289.4
S07	0.86	246.95	37350	37305	36524	25743	1332.2	1385.1	310.0
S08	0.84	245.39	35902	36224	38221	26031	1221.3	1292.5	277.6
S09	0.84	245.23	36619	36259	37441	28264	850.5	929.5	531.8
S10	0.97	257.68	42004	42074	43469	34475	1976.6	2231.8	430.7
S11	0.88	249.53	40181	38190	39551	23579	1430.3	1676.8	289.6
S12	0.90	251.25	39715	39341	38140	28738	715.7	764.0	381.5
S13	1.08	266.72	46863	46337	50223	36708	1470.7	1607.5	261.3

Table 1. Main parameters of simulated halos. $M_{\rm vir}$ is the total (dark matter plus gas) mass inside the virial radius, $r_{\rm vir}$. $N_{\rm DMO}$ and $N_{\rm DM}$ is the number of dark matter particles inside the virial radius $r_{\rm vir}$ in the "dark matter only" and "dark matter plus baryons" simulations, respectively. Columns 6 and 7 list the number of gas particles, $N_{\rm gas}$, within the virial radius and within the radius used to define the central galaxy, $r_{\rm glx} = 10$ kpc. The specific angular momentum of the dark matter within $r_{\rm vir}$ and of the baryons within $r_{\rm glx}$ is also listed.

	b/a (Dark Matter Only)			c/a (Dak Matter Only)			b/a (Dark Matter+Gas)		c/a (Dark Matter+Gas)	
	α	γ	r_α	α	γ	r_α	α	β	α	β
S02h	0.113	1.767	58.31	0.137	2.102	83.13	-0.00429	-0.00508	0.00185	-0.07127
Sample Mean Values	0.081	1.383	35.81	0.103	1.427	68.06	-0.00934	-0.01009	0.00081	-0.07220

Table 2. Best fitting parameters for isopotential contour profile shapes. Columns 1-3 (4-6) correspond to axial ratio b/a (c/a) for Dark Matter Only runs (eq. 2). Columns 7-8 (9-10) correspond to axial ratio b/a (c/a) for Dark Matter+Gas runs (eq. 3). We quote values for the high resolution run S02h shown in figure 5 and also the mean value for the sample shown as thick lines in figure 6.

Croton D. J., Springel V., White S. D. M., et al., 2006, MNRAS, 365, 11

Dubinski J., 1994, ApJ, 431, 617

Duffy A. R., Schaye J., Kay S. T., Dalla Vecchia C., 2008, MNRAS, 390, L64

Dutton A. A., Courteau S., de Jong R., Carignan C., 2005, ApJ, 619, 218

Dutton A. A., van den Bosch F. C., Courteau S., 2008, ArXiv e-prints

Dutton A. A., van den Bosch F. C., Dekel A., Courteau S., 2007, ApJ, 654, 27

Eke V. R., Navarro J. F., Steinmetz M., 2001, ApJ, 554, 114

El-Zant A., Shlosman I., Hoffman Y., 2001, ApJ, 560, 636

Frenk C. S., White S. D. M., Davis M., Efstathiou G., 1988, ApJ, 327, 507

Gnedin O. Y., Kravtsov A. V., Klypin A. A., Nagai D., 2004, ApJ, 616, 16

Gnedin O. Y., Weinberg D. H., Pizagno J., Prada F., Rix H.-W., 2007, ApJ, 671, 1115

Gustafsson M., Fairbairn M., Sommer-Larsen J., 2006, Phys Rev D, 74, 12, 123522

Hayashi E., Navarro J. F., Springel V., 2007, MNRAS, 377, 50

Jesseit R., Naab T., Burkert A., 2002, ApJL, 571, L89

Jing Y. P., Suto Y., 2002, ApJ, 574, 538

Katz N., Gunn J. E., 1991, ApJ, 377, 365

Katz N., White S. D. M., 1993, ApJ, 412, 455

Ma C.-P., Boylan-Kolchin M., 2004, Physical Review Letters, 93, 2, 021301

Meza A., Navarro J. F., Steinmetz M., Eke V. R., 2003, ApJ, 590, 619

Mo H. J., Mao S., 2004, MNRAS, 353, 829

Mo H. J., Mao S., White S. D. M., 1998, MNRAS, 295, 319

Navarro J. F., Benz W., 1991, ApJ, 380, 320

Navarro J. F., Eke V. R., Frenk C. S., 1996a, MNRAS, 283, L72

Navarro J. F., Frenk C. S., White S. D. M., 1996b, ApJ, 462, 563

Navarro J. F., Frenk C. S., White S. D. M., 1997, ApJ, 490, 493

Navarro J. F., Hayashi E., Power C., et al., 2004, MNRAS, 349, 1039

Navarro J. F., Ludlow A., Springel V., et al., 2008, ArXiv e-prints

Navarro J. F., Steinmetz M., 2000, ApJ, 538, 477

Navarro J. F., White S. D. M., 1994, MNRAS, 267, 401

Neto A. F., Gao L., Bett P., et al., 2007, MNRAS, 381, 1450

Power C., Navarro J. F., Jenkins A., et al., 2003, MNRAS, 338, 14

Reed D., Gardner J., Quinn T., et al., 2003, MNRAS, 346, 565

Sales L. V., Navarro J. F., Abadi M. G., Steinmetz M., 2007, MNRAS, 379, 1464

Sellwood J. A., 1999, in Galaxy Dynamics - A Rutgers Symposium, edited by D. R. Merritt, M. Valluri, J. A. Sellwood, vol. 182 of Astronomical Society of the Pacific Conference Series, 351–+

Sellwood J. A., McGaugh S. S., 2005, ApJ, 634, 70

Smith M. C., Ruchti G. R., Helmi A., et al., 2007, MNRAS, 379, 755

Somerville R. S., Barden M., Rix H.-W., et al., 2008, ApJ, 672, 776

Somerville R. S., Primack J. R., 1999, MNRAS, 310, 1087

Spergel D. N., Verde L., Peiris H. V., et al., 2003, ApJS, 148, 175

Springel V., White S. D. M., Jenkins A., et al., 2005, Nature, 435, 629

Wadsley J. W., Stadel J., Quinn T., 2004, New Astronomy, 9, 137

Xue X. X., Rix H. W., Zhao G., et al., 2008, ApJ, 684, 1143